1 **Effects of Electrokinetic Phenomena on Bacterial Deposition monitored by Quartz**

2 **Crystal Microbalance with Dissipation Monitoring (QCM-D)**

3

4

5 Yongping Shan[1], Lu Liu[2], Yang Liu[2], Hauke Harms[1], and Lukas Y. Wick[1]*

6

7 *[1]UFZ - Helmholtz Centre for Environmental Research, Department of Environmental*
8 *Microbiology, 04318 Leipzig, Germany.*

9 *[2] University of Alberta, Department of Civil and Environmental Engineering, 3-133*
10 *Markin/CNRL Natural Resources Engineering Facility, Edmonton, AB, T6G 2W2, Canada*
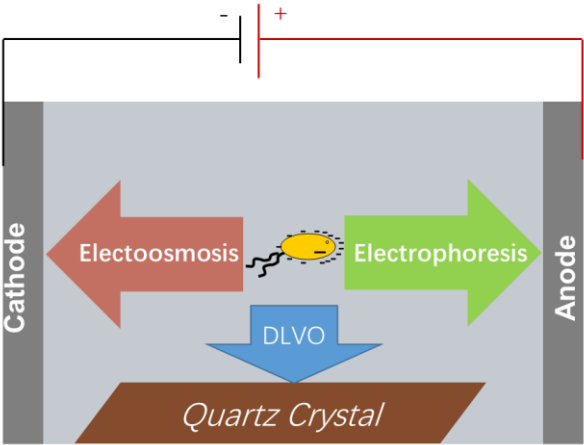
11

12

13

14

15

16 Intended for: Environmental Science & Technology

17

18

19

20

21

22

23 *Corresponding author: Mailing address: Helmholtz Centre for Environmental Research - UFZ.
24 Department of Environmental Microbiology; Permoserstrasse 15; 04318 Leipzig, Germany.
25 phone: +49 341 235 1316, fax: +49 341 235 1351, e-mail: lukas.wick@ufz.de.
26

Abstract

Bacterial deposition is the first step in the formation of microbial biofilms in environmental technology, and there is high interest in controlling such deposition. Earlier work indicated that direct electric current (DC) fields could influence bacterial deposition in percolation columns. Here, a time-resolved quartz crystal microbalance with dissipation monitoring (QCM-D) and microscopy-based cell counting were used to quantify DC field effects on the deposition of bacterial strains *Pseudomonas putida* KT2440 and *Pseudomonas fluorescens* LP6a at varying electrolyte concentrations and weak electric field strengths (0-2 V cm^{-1}). DC-induced frequency (Δf) shifts, dissipation energy (ΔD), and ratios thereof ($\Delta f/\Delta D$) proved as good indicators of the rigidity of cell attachment. We interpreted QCM-D signals using a theoretical approach calculating the attractive DLVO-force and the shear and drag forces acting on a bacterium near collector surfaces in a DC electric field. We found that changes in DC-induced deposition of bacteria depended on the relative strengths of electrophoretic drag and electroosmotic shear forces. This could enable the prediction and electrokinetic control of microbial deposition on surfaces in natural and manmade ecosystems.

Keywords: bacterial deposition, DLVO, DC electric fields, electrokinetics, electroosmosis, electrophoresis.

45 **Abstract Art**

46

47

48

Introduction

Microbial biofilms provide essential ecosystem services in many natural and manmade environments. While being beneficial in e.g. wastewater treatment systems or the degradation of contaminants, biofilms can also be detrimental to both human health and industrial applications. Biofouling can increase the corrosion of metals,[1] infect medical devices,[2,3] and pollute drinking water systems.[4–6] Direct current (DC) electric fields and their associated electrokinetic phenomena have been found to affect the bacterial deposition[7–11] that precedes biofilm formation. DC electric fields evoke various electrokinetic transport processes in both conductive[12,13] and non-conductive matrices[14,15] immersed in liquid. Electric field applied in the liquid surrounding non-conductive materials may induce electrokinetic phenomena, which allow for targeted movement of bacteria and colloidal particles in the system, even in the absence of pressure-driven hydraulic flow.[10,19–21] While electromigration and electrophoresis refer to the transport of charged molecules and particles to the electrode of opposite charge, electroosmosis reflects the surface charge-induced movement of pore fluids, usually from the anode to the cathode (electroosmotic flow, EOF).[22] Due to a plug-shaped flow profile that acts a few nanometres above a surface, EOF is thought to affect bacterial deposition by inducing shear forces (F_{EOF}).[23–25] Electrophoresis (EP), by contrast, induces a drag force (F_{EP}) on the (negatively) charged bacteria[26–28] and hence acts in the direction opposite to F_{EOF}. A bacterium approaching a surface or being located at a distance of the secondary DLVO energy minimum[29]) will be subject to F_{EOF} and F_{EP} and the relative strength of the two forces has been proposed to be a driver for observed DC field effects on bacterial deposition.[14,26,30,31] Electrokinetic phenomena are directly correlated to the electric field strength (E) applied, the surface properties of the matrices and the (bio-)colloidal particles, and the ionic strength of the electrolytes; i.e. parameters that may impact interactions between bacterium and solid surfaces.[32,33] Here we assessed the effect of DC electric fields on bacterial deposition using a

74 quartz crystal microbalance with dissipation (QCM-D) that allows for real-time

75 characterization of bacteria-surface interactions [34,35] and, hence, also electrokinetic effects on

76 bacterial deposition during transport in porous media. QCM-D reflects the amount and

77 viscoelastic properties of an adhering mass (bacteria) by changes in the resonance frequency

78 (Δf) and changes in the energy dissipation (ΔD) of an oscillating crystal coating sensor

79 surface.[36–39] The Δf is an indicator of the bacterial mass attached to the sensor while ΔD

80 indicates the softness of non-rigid mass adhesion.[40,41] Given constant temperature, liquid

81 viscosity and density, and flow velocity both signals vary according to the surface charge and

82 the hydrophobic properties of the bacteria and the sensor surface during the monitoring of

83 bacteria-surface interactions.[42–44] A plot of ΔD versus Δf compares the induced energy

84 dissipation per coupled unit mass: lower $\Delta f/\Delta D$ values indicate the formation of a dissipative,

85 soft, and fluid film, while higher $\Delta f/\Delta D$ values suggest a more rigid layer of attached bacterial

86 mass. [34,45] Hence, the Δf and ΔD of the QCM-D sensor allow to analyze the diverse responses

87 and transition from inertial to elastic loading of cells having similar surface morphologies in

88 the presence and absence of external electric fields, and hence allow to deduce the mechanisms

89 of electrokinetic effects on the surface-bacteria bond.[46,47] If Δf values are supported by direct

90 microscopy observed cell density, QCM-D monitoring can be used to quantify the rate of

91 bacterial attachment to the sensor surface, to approximate the time-resolved electrokinetic

92 effects on bacterial deposition at varying environmental conditions, and to compare bacterial

93 deposition to electrokinetically induced forces (F_{EOF} and F_{EP}) acting on bacteria adjacent to a

94 solid collector surface.

95 Here we used a QCM-D approach to assess the joint effects of a DC electric field and the ionic

96 strength of the electrolyte on the deposition at a nanogram level of two bacteria of differing

97 physicochemical cell surface properties and opposite transport behaviour in percolation

98 columns exposed to external DC fields. [14,48] QCM-D data were supported by microscopic cell

99   counting and analyzed by a recently published theoretical approach that involved calculating

100   the DLVO colloidal interaction, the hydraulic drag, and the electrokinetic forces acting on a

101   bacterium near a collector surface in a DC electric field.

102

Materials and Methods

104   **Cultivation of bacteria and inoculum preparation**

105   *Pseudomonas putida* KT2440 (GenBank accession No. AE015451)[49] and *Pseudomonas*

106   *fluorescens* LP6a (GenBank accession No. AF525494)[50] were cultivated in minimal media

107   with 1.0 gL^{-1} glucose as a carbon source until the early stationary phase (25 °C; rotary shaker

108   at 150 rpm). The cultures were then centrifuged at 3000 × g and resuspended in 10 mM (5

109   mmol K_2HPO_4 and 5 mmol KH_2PO_4 diluted in 1 L deionized water), 50 mM (29 mmol K_2HPO_4

110   and 21 mmol KH_2PO_4 diluted in 1 L DI water), and 100 mM (61 mmol K_2HPO_4 and 39 mmol

111   KH_2PO_4 diluted in 1 L DI water) potassium phosphate buffer, pH = 7 (PB) using a Vortex

112   mixer (Vortex-Genie 2, Scientific Industries, USA) to obtain bacterial suspensions with an

113   optical density at 600 nm of 0.30 ($OD_{600\ nm} = 0.30$).

114

115   **Characterization of physiochemical properties of bacterial and sensor surfaces**

116   The zeta-potentials of bacteria (ζ_{bac}) and silica beads (ζ_s) were measured by Doppler

117   electrophoretic light scattering analysis (Zetasizer Nano ZS, Malvern Instruments, Malvern,

118   UK) with a Dip Cell Kit. The zeta potential of the silica sensor surface was estimated using

119   smashed silica beads in the different electrolytes. Clean glass beads were smashed with a

120   mortar and a pestle to a size of < 100 μm, heated at 200 °C in a muffle furnace for 2 h, then

121   allowed to cool to room temperature (25 °C) under sterile conditions. The contact angles (θ) of

122   the bacterial strains and the sensor were quantified using a DSA 100 drop-shape analysis

123   system (Krüss GmbH, Hamburg, Germany) in three solvents (water, formamide, methylene

124   iodide) [15,51] and are listed in Table S1. Bacterial lawns were prepared by depositing bacteria

125   from inoculated suspensions on cellulose acetate membrane filters (Millipore, 0.45 μm); four

126   droplets were applied per filter, in triplicate experiments for each solvent.

127

128   QCM-D analysis of cell deposition on the silica sensor surface

129   Interactions between bacterial cells and a silica surface were studied with an E4 QCM-D unit

130   (Q-Sense AB, Gothenburg, Sweden) using silica-coated sensor chips (QSX-303, 5 MHz, AT-

131   cut, diameter: 14 mm, Q-Sense AB, Gothenburg, Sweden). Experiments were performed in a

132   QCM-D system comprised of an inlet solution container, four QCM-D chambers, a buffering

133   bottle, and a wastewater container (for a schematic view of the set-up cf. Fig. S1). Bacterial

134   suspensions were pumped through QCM-D tubing under pressure-driven flow using a digital

135   peristaltic pump (ISM932A, Ismatec, Cole-Parmer, Canada) at a fixed flow rate of 200 μL min^{-1}

136   (flow velocity: 6×10^{-7} m s^{-1}) at 20 ± 0.2 °C (cf. Fig. S1). DC fields ($E = 0.5$, 1.0, and 2.0 V

137   cm^{-1}) were generated by a power pack (BK Precision 9174), and connected to two Ti/Ir

138   electrodes placed in the bacterial suspension (cathode) and the anode bottle. As extensions of

139   the electrodes, two copper wires (0.2 mm i.d., renewed after each experiment) were connected

140   to the Ti/Ir electrodes. They were cautiously inserted into the tubing up to a distance of 2 mm

141   from the inlet and outlet of the QCM-D chamber, resp.; i.e. with no contact to the sensor.

142   Placement of the anode wire outside the QCM-D chamber avoided possible interferences of

143   electrochemically released copper ions with the QCM-D measurements.   Placing the copper

144   electrodes wires close to the QCM-D chamber allowed us to apply low potential while

145   simultaneously maintaining the electric field strength in the QCM-D chamber as detailed below.

146   PB at either 10, 50, or 100 mM was used as the electrolyte and DC electric fields of $E = 0$, 0.5,

147   1.0, or 2.0 V cm^{-1} were applied. Prior to the experiment, clean sterilized silica sensors were

148   mounted in the QCM-D chamber, and the screws on the back of QCM-D chambers were sealed

149 until hand-tight, then locked by the snap on the base bracket. The frequency and dissipation of

150 silica sensors in DI water were assured to deviate less than ±10% from the standard frequency

151 and dissipation values at overtones 1, 3, 5, 7, 9, 11, and 13 (corresponding to 5, 15, 25, 35, 45,

152 55, and 65 MHz), respectively. Identical ΔD and Δf signals were detected in controls pumping

153 cell-free buffer solutions in presence and absence of external DC fields. Before proceeding

154 with experiments, the system baseline was stabilized by pumping through ultrapure water for

155 20 min, followed by cell-free PB (of ionic strength equal to that of the cell suspensions) for 40

156 min. Bacterial suspensions of either *P. putida* KT2440 or *P. fluorescens* LP6a (in 10, 50, or

157 100 mM PB) were then pumped into the QCM-D chamber over 2 hours and the frequency and

158 dissipation was monitored simultaneously. Experiments were performed in triplicate at $E = 0$,

159 0.5, 1.0, and 2.0 V cm^{-1}.

160 After each experiment, the sensors were rinsed with 1.5 mL ultrapure water in a 50 mL

161 centrifuge tube and bacterial cells were detached using an ultrasonic washing unit (FS60, Fisher

162 Scientific, Canada) for 10 min. The sensor was removed using tweezers, disinfected in a UV

163 chamber for 20 min, cleaned in 50 mL of 2% sodium dodecyl sulfate (SDS), rinsed thoroughly

164 with ultrapure water, dried under a nitrogen stream, and sterilized for 20 min in a UV chamber

165 following the washing protocol provided with the silica sensors.

166

Microscopic quantification of cells attached to the sensor

168 At the end of each QCM-D analysis (i.e., after 2 h) the bacteria the cells on the sensor were

169 detached with an ultrasonic unit for 10 minutes and collected in 1.5 mL water. Detachment was

170 complete as verified by microscopic analysis of the sensor surface. The bacterial suspension

171 was centrifuged at $6000 \times g$ for 5 min, then 1.45 mL of the supernatant was removed. The

172 bacterial pellet was resuspended in the residual liquid (0.05 mL) with a Vortex mixer (Vortex-

173 Genie 2, Cole-Parmer, Canada). The suspension was then injected to a Hemacytometer

174　(Improved Neubauer 0.1 mm, Fisher Scientific, Canada) to take pictures and quantify the

175　bacterial cell concentration by epifluorescence microscopy (Axioskop II microscope, Carl

176　Zeiss, Canada) equipped with a camera (Carl Zeiss Microimaging GmbH, Canada). Pre-

177　experiments were conducted to observe the distribution of attached cells on the whole sensor

178　surface and the efficiency of ultrasonic cell detachment, resp. Images were analyzed by ImageJ

179　software (ImageJ 1.46r, USA) to quantify the cells. The automatic counting codes used for cell

180　counting are listed in the supporting information. The density of the cells removed from the

181　sensor surface (d_c) was calculated by dividing the number of cells detached from each sensor

182　by the sensor surface area.

183

184

Theory

Forces acting on bacteria on a collector surface

187　Although the Derjaguin, Landau, Verwey, and Overbeek (DLVO) theory of colloidal

188　interactions[52–54] does not account for surface heterogeneity, hydration effects, or hydrophobic

189　interactions, it is a powerful predictor of bacterial deposition in solutions of high ionic strength

190　($I = 0.1$-0.3 M).[29,55–57] DLVO interaction energy profiles of bacterial deposition depend on the

191　physicochemical properties of the microbe, the collector surface, and the ionic strength of the

192　aqueous medium. DLVO theory also predicts reversible bacterial deposition even at high

193　attractive forces[58,59] at a so-called secondary minimum of the energy profile, typically located

194　5-20 nm above a collector surface. Therefore, net forces acting on bacteria in the secondary

195　minimum may influence bacterial deposition, bacterial attachment, and biofilm formation.[14,15]

196　The net force at the secondary minimum is estimated to act on a bacterium through a

197　combination of the DLVO force of colloidal interaction (F_{DLVO}), the hydraulic flow shear force

198   (F_{HF}), the electroosmotic flow shear force (F_{EOF}), and the electrophoretic drag force (F_{EP}),[14] as

199   shown in Eq. 1:

200    $$F_{net} = F_{DLVO} + F_{HF} + F_{EOF} + F_{EP}.$$ (1)

201   The DLVO interaction force and hydraulic force are depicted in Eqs. S1-S11. It should be noted

202   that the DLVO force is calculated at the secondary minimum distance, where the DLVO

203   interaction controls the reversible bacterial deposition.[59] The electroosmotic shear force can be

204   calculated with Eq. 2:

205    $$F_{EOF} = F_d^* \times 6\pi\eta a V_{EOF} = F_d^* \times 6\pi\eta a \times [-\frac{\varepsilon_0\varepsilon_r\xi_s E}{\eta}(1 - \frac{2I_1(\kappa h_s)}{\kappa a I_0(\kappa h_s)})],$$ (2)

206   where F_d^* is a function of the radius a of a sphere (for simplicity we consider bacterial cells to

207   be spheres); the distance of the center of the sphere to the collector surface, F_d^*, is estimated

208   to be 1.7; η is the viscosity of the liquid (η = 3.19 kg m^{-1} h^{-1}), ε_r is the dielectric constant of

209   water (78.5), ε_0 (8.85 $\times$ 10^{-12} F m^{-1}) is the dialectic permittivity in vacuum, ζ_s is the zeta

210   potential of the sensor surface in the experimental conditions, and E is the electric field strength

211   applied. I_0 and I_1 are zero-order and first-order modified Bessel functions, and κ^{-1} is the

212   thickness of the electric double layer. The electrophoretic drag force F_{EP} follows the

213   Smoluchowski equation (Eq. 3):

214    $$F_{EP} = 6\pi\eta a V_{EP} = 6\pi\eta a \times \frac{2\varepsilon_0\varepsilon_r\xi_{bac}E}{3\eta} f(\kappa a),$$ (3)

215   where ζ_{bac} is the zeta potential of the bacteria at the given experimental conditions; $f(\kappa a)$ values

216   approach 1.5 at high electrolyte concentration (i.e., 50 and 100 mM); and $f(\kappa a)$ is close 1.0 at

217   low ionic strength (i.e., 10 mM) for the bacterial radius a = 0.6 μm.[22] The ratio $|F_{EOF}|/|F_{EP}|$ at

218   the secondary minimum of the DLVO interaction energy above a collector surface (h_s) is

219   expressed in Eq. 4:

220
$$\frac{|F_{EOF}|}{|F_{EP}|} = \frac{F_d^* \xi_s}{\frac{2}{3}\xi_{bac}f(\kappa a)}[1 - \frac{2I_1(\kappa h_s)}{\kappa a I_0(\kappa h_s)}].$$
(4)

221 Eq. 4 indicates that the $|F_{EOF}|/|F_{EP}|$ ratio depends on ζ_{bac}, ζ_s, and the thickness of the electric

222 double layer κ^{-1}, and is therefore strongly influenced by the ionic strength of the electrolyte.

223

224 **QCM-D analyses of bacterial deposition**

225 QCM-D is an acoustic method that reflects the amount and viscoelastic properties of an

226 adhering mass by changes in the resonance frequency (Δf) and energy dissipation (ΔD) of an

227 oscillating crystal-coated sensor surface.[36–39 60,61] The change in resonance frequency, Δf, can

228 be described by the Sauerbrey equation in case of rigid attachment and negative Δf:[62]

229
$$\Delta f = \frac{-2f_0^2 \Delta m}{A\sqrt{\rho_q \mu_q}} = -C_f \Delta m,$$
(5)

230 where f_0 denotes the fundamental resonance frequency, A is the electrode area, ρ_q is the density

231 of quartz ($\rho_q = 2.648$ g cm^{-3}), and μ_q is the shear modulus of quartz ($\mu_q = 2.957 \times 10^{10}$ N m^{-2}).

232 The $\Delta f/\Delta D$ ratio indicates changes in energy dissipation per coupled unit mass and indicates

233 the rigidity and attachment strength of bacterial adhesion.[45,47,63] Typically, bacterial adhesion

234 leads to a negative frequency shift and a positive dissipation shift. Thus, a low negative $\Delta f/\Delta D$

235 value indicates the buildup of a dissipative soft and fluid film on the QCM-D sensor. In contrast,

236 higher negative values of $\Delta f/\Delta D$ indicate a more rigid layer.

237

238 **Results**

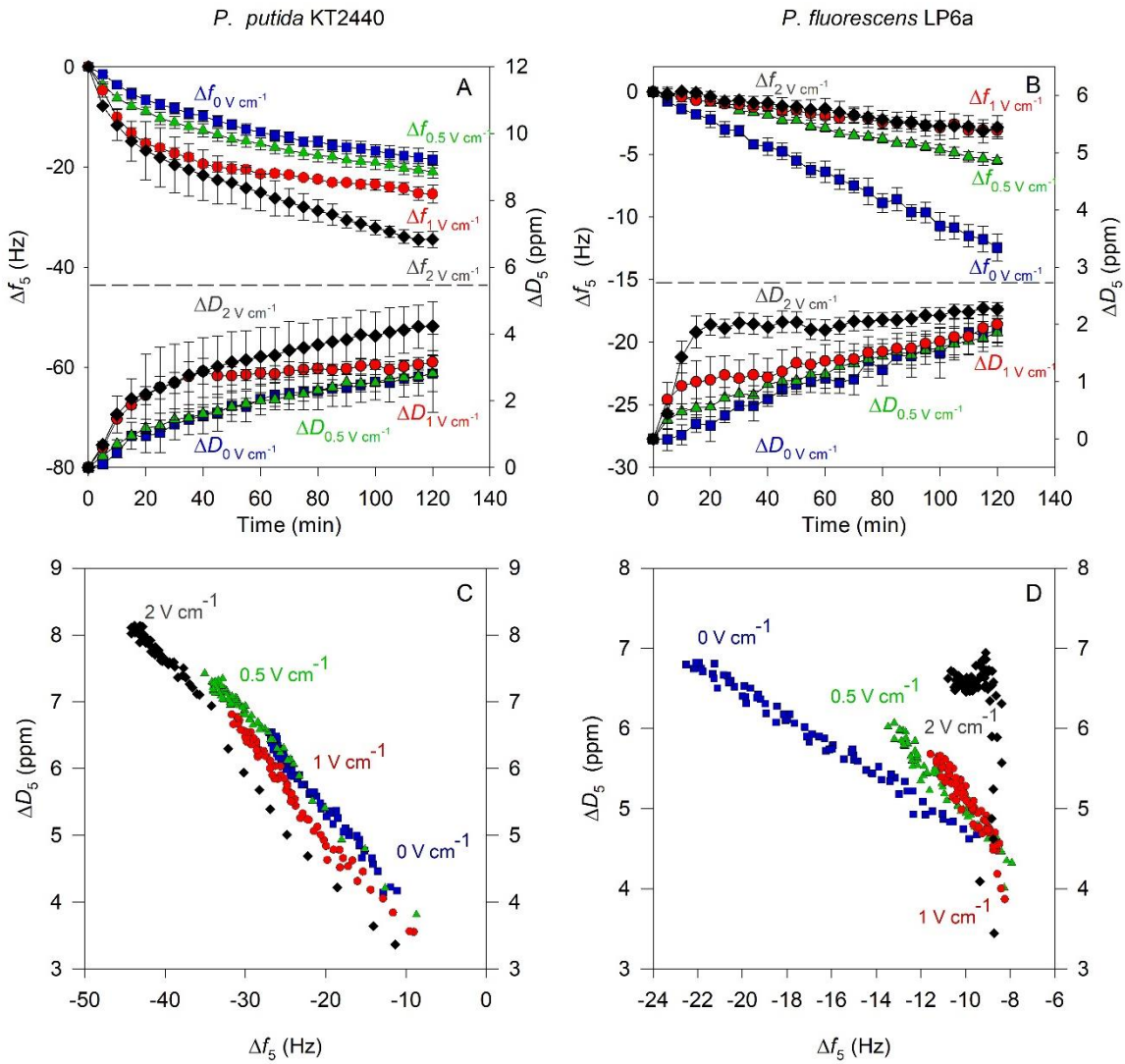239 **Electric field effects and electrolyte effects on the calculated F_{net}**

240 In order to approximate the DLVO energy profiles and the electrokinetic forces acting on

241 bacteria above a sensor surface, the physicochemical properties of the sensor surface and the

242 bacteria were determined in 10, 50, and 100 mM PB solutions. While the quartz sensor was

243 hydrophilic (water contact angle, $\theta_{w,}$ = 21°), both bacterial strains were moderately

244 hydrophobic ($\theta_{w,KT2440}$ = 70°; $\theta_{w,LP6a}$ = 46°; Table S1). The sensor surface and both bacterial

245 strains were negatively charged in all PB concentrations (Table 1), with more negative zeta

246 potentials at lower ionic strengths (i.e. shifts from –21 mV (10 mM PB) to –8 mV (100 mM

247 PB) of the sensor, -30 mV to –11 mV (strain KT2440) and –53 mV to –36 mV (strain LP6a)

248 (Table 1). Calculated DLVO interaction energy profiles between the bacteria and the QCM-D

249 quartz sensor surfaces (Fig. S2) all exhibited secondary minima, suggesting reversible bacteria

250 attachment at all PB concentrations. Secondary minima were found at separation distances of

251 3.2 – 20.6 nm (Table S2). Corresponding attractive DLVO forces (F_{DLVO}) depended on the ionic

252 strength of the PB and ranged from 0.15 pN (10 mM) to 3.26 pN (100 mM) for strain KT2440

253 and from 0.15 pN (10 mM) to 2.31 pN (100 mM) for strain LP6a (Table 1). Table 1 summarizes

254 the magnitudes of the forces F_{HF}, F_{EOF}, F_{EP}, and F_{net} that we defined as the sum of the

255 magnitudes of F_{HF}, F_{EOF}, and F_{EP}, and F_{DLVO}, disregarding distinct directions of electrokinetic

256 and DLVO forces (Eq. 1). As sensor and bacterial surfaces had negative zeta potentials (Table

257 1), the direction of F_{EP} was opposed to the direction of F_{EOF}, and the magnitudes of F_{EP} were of

258 opposite sign to the magnitudes of F_{EOF}. While the extent of F_{HF} was assumed to be independent

259 of experimental variations, the magnitudes of F_{EOF} and F_{EP} (expressed by $|F_{EOF}|$ and $|F_{EP}|$)

260 increased proportionally to E (Eqs. 2 and 3), and decreased at rising electrolyte concentrations.

261 F_{net} thus depended on the electric field strength and the ionic strength of the PB (Table 1): at

262 any given electric field strength, higher PB concentrations increased the F_{net} of both bacterial

263 strains. At a given ionic strength, however, the F_{net} of the two bacterial strains revealed

264 dissimilar trends at increasing E: in 50 mM and 100 mM PB; an increase in E from 0.5 V cm^{-1}

265 to 2 V cm^{-1} increased F_{net} by ca. 10-20% for strain KT2440 and decreased F_{net} by ca. 700%
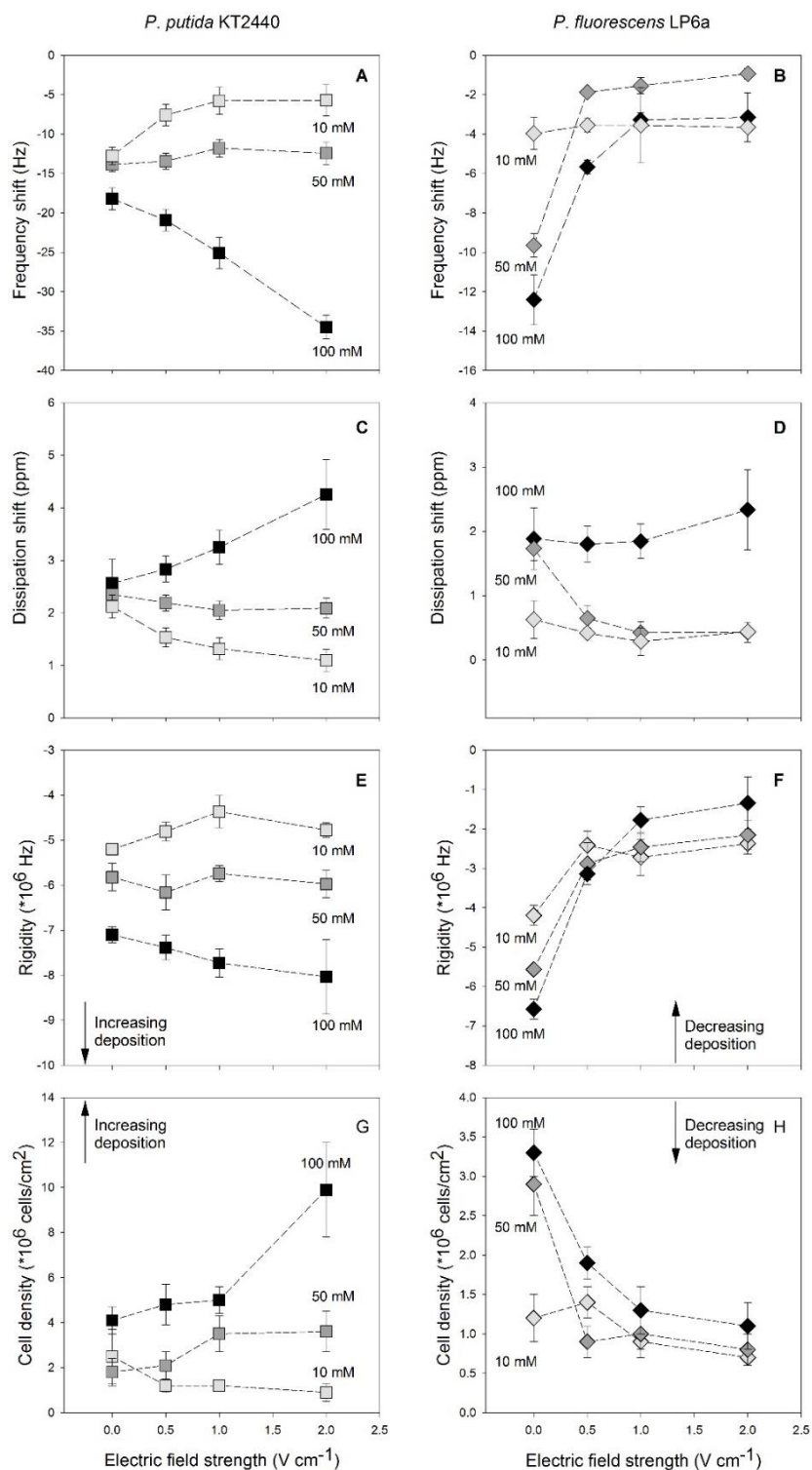
266 for strain LP6a (Table 1).

267 **Table 1.** Overview of cell density, zeta potential, and the calculated forces acting on a bacterium (*P.*
268 *putida* KT2440 or *P. fluorescens* LP6a) at a distance of the secondary minimum in the presence and
269 absence of a DC electric current at different electrolyte strengths.

270

		P. putida KT2440				*P. fluorescens* LP6a		
		10 mM	50 mM	100 mM		10 mM	50 mM	100 mM
DLVO force (pN) [a]	F_{DLVO}	0.15	1.45	3.26		0.15	1.43	2.31
Hydraulic shear force (pN) [b]	F_{HF}	0.50	0.50	0.50		0.50	0.50	0.50
Electroosmotic shear force per V cm^{-1} (pN)	F_{EOF}	3.70	1.90	1.80		3.70	1.90	1.80
Electrophoretic drag force per V cm^{-1} (pN)	F_{EP}	-3.95	-1.80	-1.45		-6.99	-5.69	-4.74
Net force (pN) [c]								
$E = 0$ V cm^{-1}	$F_{net,ND}$	0.65	1.95	3.76		0.65	1.93	2.81
$E = 0.5$ V cm^{-1}	$F_{net,0.5V\,cm^{-1}}$	0.53	2.00	3.94		-1.00	0.03	1.34
$E = 1$ V cm^{-1}	$F_{net,1V\,cm^{-1}}$	0.40	2.05	4.11		-2.65	-1.86	-0.13
$E = 2$ V cm^{-1}	$F_{net,2V\,cm^{-1}}$	0.15	2.15	4.46		-5.95	-5.65	-3.07
Cell density (10^6 cells cm^{-2}) [d]	d_c							
$E = 0.0$ V cm^{-1}	$d_{c,\,no\,DC}$	2.5 ± 0.2	1.8 ± 0.6	4.1 ± 0.6		1.4 ± 0.2	2.9 ± 0.4	3.3 ± 0.3
$E = 0.5$ V cm^{-1}	$d_{c,\,0.5V\,cm^{-1}}$	1.2 ± 0.3	2.1 ± 0.6	4.8 ± 0.9		1.2 ± 0.3	0.9 ± 0.2	1.9 ± 0.2
$E = 1$ V cm^{-1}	$d_{c,\,1V\,cm^{-1}}$	1.2 ± 0.2	3.5 ± 0.8	5.0 ± 0.6		0.9 ± 0.1	1.0 ± 0.3	1.3 ± 0.3
$E = 2$ V cm^{-1}	$d_{c,\,2V\,cm^{-1}}$	0.9 ± 0.4	3.6 ± 0.9	9.9 ± 2.1		0.7 ± 0.1	0.8 ± 0.2	1.1 ± 0.3
Zeta potential (-mV)								
Bacteria	ζ_{bac}	-30 ± 1	-14 ± 2	-11 ± 1		-53 ± 2	-43 ± 2	-36 ± 3
		Sensor surface						
Silica [e]	ζ_s	-21 ± 2	-12 ± 1	-8 ± 1				

271 [a] For calculation cf. Eq. S10; [b] F_{HF} calculated for flow velocity of 6×10^{-7} m s^{-1} (cf. Eq. S11); [c] cf. Eq. 1; [d] Microscopically
272 determined cell density after 2 h; [e] Silica sensor surface.

Figure 1. Time dependent frequency shifts (Δf_5) and dissipation shifts (ΔD_5) of *P. putida* KT2440 (Fig. 1A) and *P. fluorescens* LP6a (Fig. 1B) at overtone 5 in 100 mM PB and electric field strengths of $E = 0$ V cm^{-1} (blue squares), $E = 0.5$ V cm^{-1} (green triangles), $E= 1.0$ V cm^{-1} (red circles), and $E = 2.0$ V cm^{-1} (black diamonds). Error bars denote the standard deviation of the mean ($n = 3$). Data above and below the dashed line refer to Δf_5 (left y-axis) and to ΔD_5 (right y-axis), respectively. Panels C and D correlate the time dependent ΔD_5 and Δf_5 of *P. putida* KT2440 and *P. fluorescens* LP6a.

14

P. putida KT2440   P. fluorescens LP6a

281

282

Figure 2. Effect of the electric field strength on the frequency shift (Δf_5; Figs. 2A and 2B), the dissipation shift (ΔD_5; Figs 2C and 2D), the rigidity of bacterial attachment ($\Delta f_5/\Delta D_5$, Figs. 2E and 2F), and the cell density on the sensor surface (Figs. 2G and 2H). Bacterial deposition of *P. putida* KT2440, Figs. 2A, 2C, 2E, and 2G, and *P. fluorescens* LP6a, Figs. 2B, 2D, 2F, and 2H, after two hours (cf. Fig. S3) at overtone 5 in 10 mM (light gray), 50 mM (dark gray) and 100 mM (black) PB.

15

Electric field and electrolyte effects on Δf and ΔD and derived cell attachment rigidity

QCM-D experiments recorded frequency shifts and dissipation shifts at overtones 1, 3, 5, 7, 9, 11, and 13 (Fig. S3) during 120 minutes of bacterial deposition. While overtone 1 was poorly stable and overly sensitive, all other overtones showed similar trends (Figs. S4 and S5). In the following, we analyze and discuss overtone 5 as a representative signal using the frequency/dissipation baseline in cell-free PB as a reference to calculate the frequency and dissipation shifts of the bacteria deposition (Figs. 1, S4, and S5). Figure 1 exemplifies Δf_5 and ΔD_5 shifts of both strains in 100 mM PB at electric field strengths of $E = 0$, 0.5, 1, and 2 V cm^{-1}. Here, pumping bacteria over the sensor surface resulted in a decrease in frequency shifts and an increase in dissipation shifts; Δf_5 and ΔD_5 varied at different experimental conditions (Figs. 1A, 1B, S4, and S5). Generally, the rates of Δf_5 and ΔD_5 were higher at the beginning (0-15 minutes) of bacterial deposition than at the end of bacterial deposition (Figs. 1A, 1B for 100 mM PB and Figs. S4, S5 for 10 and 50 mM PB), while the ratio $\Delta f_5/\Delta D_5$, an indicator of attachment rigidity, generally exhibited a linear correlation with Δf_5 and ΔD_5 ranges, with coefficients of determination (r^2) of > 0.95 (Figs. 1C, 1D, Table S4). Figs. 2A-F summarize Δf_5, ΔD_5, and $\Delta f_5/\Delta D_5$ ratios at the end of the deposition experiments. While signals of strains KT2440 and LP6a differed depending on the experimental conditions, the effects observed were proportional to the electric field strength applied; i.e., a higher voltage resulted in stronger observed effects. For strain KT2440 in 100 mM PB, for instance, Δf_5 decreased from -18.2 Hz ($E = 0$ V cm^{-1}) to -34.5 Hz ($E = 2.0$ V cm^{-1}) while ΔD_5 increased from 2.56 ppm to 4.25 ppm (Figs. 2A and 2 C). Such shifts resulted in clear increases in the calculated rigidity (i.e., more negative $\Delta f_5/\Delta D_5$ ratios; Fig. 2E). In contrast, Δf_5, ΔD_5, and $\Delta f_5/\Delta D_5$ ratios of strain LP6a in 100 mM PB increased with increasing electric field strengths; i.e., Δf_5 from -12.4 Hz to -3.14 Hz, ΔD_5 from 1.89 ppm to 2.34 ppm, and $\Delta f_5/\Delta D_5$ from -6.56 to -1.34 MHz (Figs. 2 B, D, F). Decreasing PB concentrations from 100 mM to 10 mM resulted in lower shifts of Δf_5, ΔD_5,

313   and $\Delta f_5/\Delta D_5$ in DC free controls and smaller DC-induced changes, respectively. For strain LP6a,

314   an electric field as weak as $E = 0.5$ V cm^{-1} resulted in distinct changes in Δf_5, ΔD_5, and $\Delta f_5/\Delta D_5$

315   at all PB concentrations. In contrast, DC field effects on the trends of Δf_5, ΔD_5, and $\Delta f_5/\Delta D_5$ of

316   strain KT2440 varied with the concentration of the electrolyte. At PB concentrations of 10 and

317   50 mM, DC fields decreased the rigidity of attached KT2440 cells, while more negative

318    $\Delta f_5/\Delta D_5$ ratios (i.e., more rigid attachments) were observed at increasing E.

Electric field and electrolyte effects on cell density of attached bacteria

320   The number of cells attached to the sensor surface was counted microscopically at the end of

321   the deposition experiments. The cell density (d_c) and the surface coverage (cf. Eq. S12) of cells

322   attached to the quartz sensor surface (1.54 cm^2) were approximated. The d_c varied from $0.9 \times$

323   10^6 to 9.9×10^6 cells cm^{-2} (strain KT2440) and from 0.7×10^6 to 3.3×10^6 cells cm^{-2} (strain

324   LP6a) (Table 1; Figs. 2G and 2H). This corresponds to maximal coverages of the sensor surface

325   (Table S3) of 5.5% and 1.8%, respectively. In strain LP6a (where d_c at 10 mM and 50 mM

326   were similar), the cell density increased in the order of d_c (10 mM) $< d_c$ (50 mM) $< d_c$ (100

327   mM) at all electric field strengths (Table 1). At a given PB concentration, however, the strength

328   of the electric fields evoked distinct d_c differences between the two bacterial strains (Table 1

329   and Figs. 2E and 2F). An increase in E resulted in a decrease in the d_c of strain LP6a at all

330   electrolyte concentrations, suggesting that DC electric fields reduced the deposition of LP6a

331   cells to the sensor surface even at weak E. For strain KT2440 however, an increase in the

332   electric field decreased cell attachment to the sensor in 10 mM PB, but promoted cell

333   attachment in 50 mM and 100 mM PB (Table 1 and Figs. 2E and 2F). Cell density data for both

334   bacterial strains thereby showed similar relative trends in Δf_5 and ΔD_5 (Figs. 2A, 2B).

335

336

17

Discussion

Assessment of DC-induced deposition effects by QCM-D monitoring
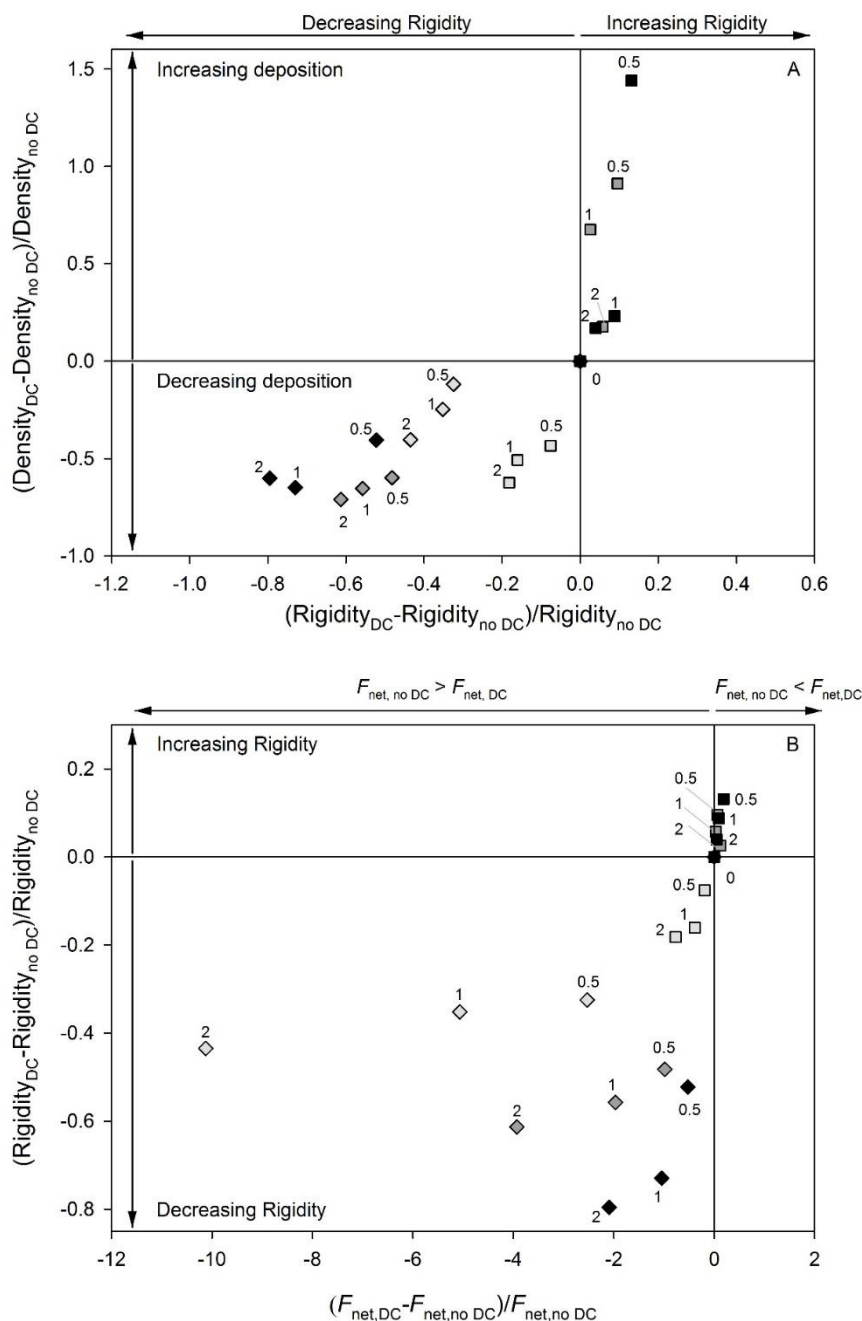
Motivated by recent work that suggested that bacterial deposition and transport in percolation systems is influenced by electrokinetic forces,[14] we studied DC electric field effects on bacterial deposition using real-time QCM-D monitoring at varying PB concentrations (10-100 mM) and electric field strengths (0-2 V cm^{-1}). Electrolyte concentration and electric field strength are key drivers of electrokinetic shear and drag forces acting on bacteria. QCM-D signals were further compared to cell density. The results are discussed based on approximations of the net force (F_{net}; Eq. 1) acting on a bacterium at the distance of reversible attachment (i.e., at the secondary minimum of the DLVO interaction energy of bacterial adhesion, G_{DLVO}, Eq. S1 and Fig. S2). Except for strain LP6a at 2 V cm^{-1}, we found good correlation between the resonance frequency (Δf_5) and the dissipation energy (ΔD_5) in bacterial strains KT2440 and LP6a in all experiments (Figs. 1C and 1D). Based on work by Gutman et al.,[45] we used $\Delta f_5/\Delta D_5$ ratios to indicate attachment rigidity[42] and cell deposition.[34] Our data showed good correlation between $\Delta f_5/\Delta D_5$ and the microscopically determined cell density (d_c). (Fig. 3A). Backed by both the attachment rigidity and the cell density, we found that weak DC fields clearly changed the deposition patterns of strains KT2440 and LP6a compared to DC-free controls (Figs. 2E-2H). Observed deposition effects were proportional to the electric field strength applied (i.e., stronger effects were exhibited at higher E), yet were dependent on the bacterial cell surface properties and the PB ionic strength (Fig. 2).

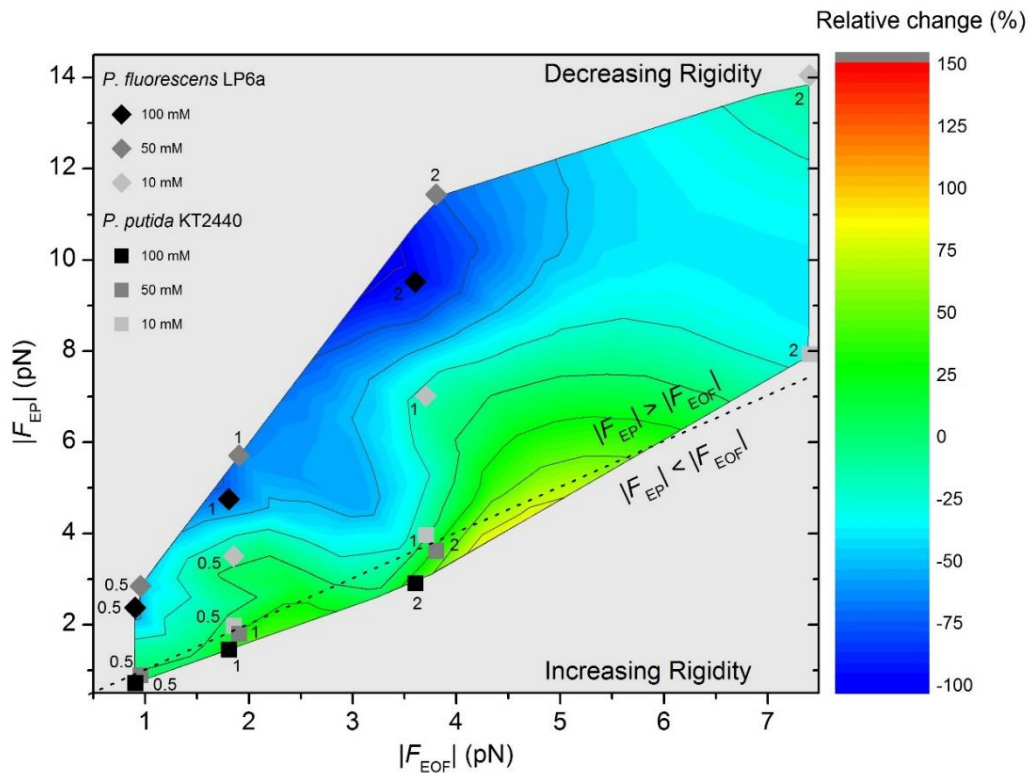**Prediction of DC-induced bacterial deposition effects**

According to the Derjaguin, Landau, Verwey, and Overbeek (DLVO) theory,[53] deposition of a bacterium to a sensor surface requires that the net kinetic energy of the bacterium is lower than the DLVO interaction energy at the distance of reversible attachment.[56,64] Prediction of DC

361   electric field effects on bacterial deposition should therefore consider additional electrokinetic

362   forces acting on depositing cells; for example, electroosmotic shear and electrophoretic drag

363   forces have powerful effects on the movement of bacteria and (bio-)colloidal particles.[7,9,16] We

364   correlated DC-induced deposition effects with F_{net} shifts (Figs. 3B and S7); i.e., the attachment

365   rigidity ($\Delta f_5/\Delta D_5$) and the cell density (d_c) were correlated with the F_{net} acting on a bacterium

366   at the secondary minimum above the sensor surface. For easier comparison, all data were

367   normalized for DC-free controls, using $((\Delta f_5/\Delta D_5)_{DC} - (\Delta f_5/\Delta D_5)_{no\ DC}/(\Delta f_5/\Delta D_5)_{no\ DC})$ i.e.: for

368   attachment rigidity, $(d_{c,DC} - d_{c\ no\ DC})/(d_{c,no\ DC})$ for cell density, and $(F_{net,DC} - F_{net,no\ DC})/F_{net,no\ DC}$

369   for normalized net force shifts, respectively. In doing so, we found good correlation between

370   the normalized d_c and QCM-D derived rigidity (Fig 3A) at all electric field strengths and buffer

371   concentrations tested. Increasing attachment rigidity was mirrored by higher d_c, while

372   decreasing attachment rigidity resulted in lower d_c (Fig. 3A). This highlights QCM-D as a

373   useful approach to assess and predict the influence of DC electric fields on bacterial deposition:

374   At $F_{net,DC} > F_{net,noDC}$, increased attachment rigidity (Fig 3B) and higher d_c (Fig. S7) were

375   observed, and at $F_{net,DC} < F_{net,noDC}$, lower attachment rigidity (Fig 3B) and lower d_c (Fig. S7)

376   were observed. As F_{EOF} and F_{EP} are of opposite sign in our experimental system, their relative

377   strengths are a driver of $F_{net,DC}$ (Eq. 1) and, thus, of observed electrokinetic effects on bacterial

378   deposition (Figs. 4 and S8). If $|F_{EOF}| > |F_{EP}|$, DC fields promote attachment rigidity and d_c and

379   *vice versa*, respectively.[14] Therefore, $|F_{EOF}|/|F_{EP}|$ was a good predictor of bacterial electrokinetic

380   effects on cell attachment rigidity and bacterial deposition in all conditions tested. The heat

381   maps in Figs. 4 and S8 show the effects of $|F_{EOF}|$ and $|F_{EP}|$ on the normalized DC-induced

382   rigidity and d_c changes. They reveal the importance of $|F_{EP}|$ for cell deposition at a given $|F_{EOF}|$,

383   independent of bacterial strain, electrolyte strength, and applied electric field. The high degree

384   of convergence between changes in rigidity and changes in d_c further indicates that QCM-D is

385   a useful and expedient tool for the real-time analysis of electrokinetic deposition.

386

387   **Figure 3**. Correlation of normalized changes in DC-induced cell density, rigidity of cell attachment
388   (Fig. 3A), DC-induced net force ($F_{net,DC}$, cf. Eq. 1), and rigidity of cell attachment (Fig. 3B), respectively.
389   All plots reflect data after two hours of deposition of *P. putida* KT2440 (squares) and *P. fluorescens*
390   LP6a (diamonds) exposed to PB at concentrations of 10 mM (light gray), 50 mM (dark gray), and 100
391   mM (black), and DC electric field strengths of $E = 0$, 0.5, 1.0, or 2.0 V cm^{-1} (cf. digits at the symbols).

392

Figure 4. Calculated effects of the electroosmotic shear force $|F_{EOF}|$ and the electrophoretic drag force $|F_{EP}|$ on DC-induced normalized changes in the rigidity of cell attachment after two hours of deposition of *P. putida* KT2440 (squares) and *P. fluorescens* LP6a (diamonds). Experiments were performed in PB at concentrations of 10 mM (light gray), 50 mM (dark gray), and 100 mM (black), and DC electric field strengths of $E = 0$, 0.5, 1.0, or 2.0 V cm^{-1} (cf. digits at the symbols). Data points above the dashed line (i.e. $|F_{EP}| > |F_{EOF}|$) and below the dashed line (i.e. $|F_{EP}| < |F_{EOF}|$) refer to decreased and increased rigidity, respectively, compared to DC-free controls.

Relevance of findings to environmental applications

Electrokinetic transport processes are often applied in civil and environmental engineering such as for wood preservation or for contaminant removal. As an alternative to physical filtration, electrokinetic approaches can be used to pre-concentrate large molecules and nanoparticles using the double layer properties of nanochanels ("electrokinetic trapping"[65]). Here we applied electrokinetic forces to influence bacterial deposition on surfaces. Electrokinetic deposition approaches may be used in future applications to retain unwanted bacteria in drinking water purification systems or - vice versa - to reduce bacterial deposition and subsequent bio-fouling in engineered systems. . The relative strength of F_{EOF} and F_{EP} acting on bacteria at a distance of

21

the secondary DLVO minimum above a surface was found to be a good predictor of

electrokinetic effects on cell deposition. According to Eq. 4, the $|F_{EOF}|/|F_{EP}|$ ratio is influenced

by the electric field strength, the ionic strength of the electrolyte, the zeta potentials of bacteria

and bacteria collector surfaces, and the thickness of the electric double layer. QCM-D allows

for fast, real-time and accurate high throughput monitoring of bacterial deposition by easily

changing the drivers of the $|F_{EOF}|/|F_{EP}|$ ratio. It can be used to predict electrokinetic effects on

bacterial deposition in environmental and biotechnological applications (e.g., elimination of

unwanted bacteria in drinking water or the prevention of biofilm induced corrosion).

Knowledge on DC-effects also allows to manage electrokinetic bacterial dispersal in

subsurface porous media and e.g. to change microbial community structures and functions and

to promote contaminant biodegradation in disturbed ecosystems.[66,67] Electrokinetic effects may

also improve the transport of nutrients by electromigration or change the interactions of

contaminants with sorbents,[68,69] thereby enhancing the biodegradation of contaminants during

engineered clean-up of contaminated soil or waters.

Supporting Information. The SI contains 4 tables and 8 figures as well as calculations of the

DLVO interaction force between bacteria and a solid surface (F_{DLVO}), and the hydraulic shear

force F_{HF}, resp. It further describes the estimation of the bacterial coverage of attached bacterial

cells on the sensor and provides a code for ImageJ automatic cell counting of images taken

with a Hemacytometer.

Reference

(1)   Iverson, W. P. Microbial Corrosion of Metals. In *Advances in Applied Microbiology*; Laskin, A. I., Ed.; Academic Press, 1987; Vol. 32, pp 1–36. https://doi.org/10.1016/S0065-2164(08)70077-7.

(2)   Russotto, V.; Cortegiani, A.; Raineri, S. M.; Giarratano, A. Bacterial Contamination of Inanimate Surfaces and Equipment in the Intensive Care Unit. *J. Intensive Care* **2015**, *3* (1), 54. https://doi.org/10.1186/s40560-015-0120-5.

(3)   Fafliora, E.; Bampalis, V. G.; Lazarou, N.; Mantzouranis, G.; Anastassiou, E. D.; Spiliopoulou, I.; Christofidou, M. Bacterial Contamination of Medical Devices in a Greek Emergency Department: Impact of Physicians' Cleaning Habits. *Am. J. Infect. Control* **2014**, *42* (7), 807–809. https://doi.org/10.1016/j.ajic.2014.03.017.

(4)   Douterelo, I.; Jackson, M.; Solomon, C.; Boxall, J. Microbial Analysis of in Situ Biofilm Formation in Drinking Water Distribution Systems: Implications for Monitoring and Control of Drinking Water Quality. *Appl. Microbiol. Biotechnol.* **2016**, *100* (7), 3301–3311. https://doi.org/10.1007/s00253-015-7155-3.

(5)   Lamka, K. G.; Lechevallier, M. W.; Seidler, R. J. Bacterial Contamination of Drinking Water Supplies in a Modern Rural Neighborhoodt. *APPL Env. MICROBIOL* **1980**, *39*, 5.

(6)   *Guidelines for Drinking-Water Quality*, 4th ed.; World Health Organization, Ed.; World Health Organization: Geneva, 2011.

(7)   Masliyah, J. H.; Bhattacharjee, S. *Electrokinetic and Colloid Transport Phenomena*; John Wiley & Sons: New Jersey, 2006.

(8)   *Interfacial Electrokinetics and Electrophoresis*; Delgado, Á. V., Ed.; Surfactant science series; Marcel Dekker, Inc: New York, 2002.

(9)   Shi, L.; Müller, S.; Harms, H.; Wick, L. Y. Factors Influencing the Electrokinetic Dispersion of PAH-Degrading Bacteria in a Laboratory Model Aquifer. *Appl. Microbiol. Biotechnol.* **2008**, *80* (3), 507–515. https://doi.org/10.1007/s00253-008-1577-0.

(10) Shi, L.; Müller, S.; Harms, H.; Wick, L. Y. Effect of Electrokinetic Transport on the Vulnerability of PAH-Degrading Bacteria in a Model Aquifer. *Environ. Geochem. Health* **2008**, *30* (2), 177–182. https://doi.org/10.1007/s10653-008-9146-0.

(11) Wick, L. Y.; Shi, L.; Harms, H. Electro-Bioremediation of Hydrophobic Organic Soil-Contaminants: A Review of Fundamental Interactions. *Electrochimica Acta* **2007**, *52* (10), 3441–3448. https://doi.org/10.1016/j.electacta.2006.03.117.

(12) Pandit, S.; Shanbhag, S.; Mauter, M.; Oren, Y.; Herzberg, M. Influence of Electric Fields on Biofouling of Carbonaceous Electrodes. *Environ. Sci. Technol.* **2017**, *51* (17), 10022–10030. https://doi.org/10.1021/acs.est.6b06339.

(13) Gall, I.; Herzberg, M.; Oren, Y. The Effect of Electric Fields on Bacterial Attachment to Conductive Surfaces. *Soft Matter* **2013**, *9* (8), 2443–2452. https://doi.org/10.1039/C2SM27270A.

(14) Shan, Y.; Harms, H.; Wick, L. Y. Electric Field Effects on Bacterial Deposition and Transport in Porous Media. *Environ. Sci. Technol.* **2018**, *52* (24), 14294–14301. https://doi.org/10.1021/acs.est.8b03648.

(15) Qin, J.; Sun, X.; Liu, Y.; Berthold, T.; Harms, H.; Wick, L. Y. Electrokinetic Control of Bacterial Deposition and Transport. *Environ. Sci. Technol.* **2015**, *49* (9), 5663–5671. https://doi.org/10.1021/es506245y.

(16) Hunter, R. J. *Zeta Potential in Colloid Science: Principles and Applications*, 3. print.; Colloid science; Academic Pr: London, 1988.

(17) Hu, Y.; Werner, C.; Li, D. Electrokinetic Transport through Rough Microchannels. *Anal. Chem.* **2003**, *75* (21), 5747–5758. https://doi.org/10.1021/ac0347157.

(18) Kuo, C. C.; Papadopoulos, K. D. Electrokinetic: Movement of Settled Spherical Particles in Fine Capillaries. *Environ. Sci. Technol.* **1996**, *30* (4), 1176–1179. https://doi.org/10.1021/es950413d.

487   (19) Wick, L. Y.; Mattle, P. A.; Wattiau, P.; Harms, H. Electrokinetic Transport of PAH-Degrading
488   Bacteria in Model Aquifers and Soil. *Environ. Sci. Technol.* **2004**, *38* (17), 4596–4602.
489   https://doi.org/10.1021/es0354420.
490   (20) Secord, E. L.; Kottara, A.; Van Cappellen, P.; Lima, A. T. Inoculating Bacteria into Polycyclic
491   Aromatic Hydrocarbon-Contaminated Oil Sands Soil by Means of Electrokinetics. *Water. Air.*
492   *Soil Pollut.* **2016**, *227* (8), 288.
493   (21) Haber, S. Deep Electrophoretic Penetration and Deposition of Ceramic Particles inside
494   Impermeable Porous Substrates. *J. Colloid Interface Sci.* **1996**, *179* (2), 380–390.
495   (22) Elimelech, M. Particle Deposition on Ideal Collectors from Dilute Flowing Suspensions:
496   Mathematical Formulation, Numerical Solution, and Simulations. *Sep. Technol.* **1994**, *4* (4),
497   186–212. https://doi.org/10.1016/0956-9618(94)80024-3.
498   (23) Ross, D.; Johnson, T. J.; Locascio, L. E. Imaging of Electroosmotic Flow in Plastic
499   Microchannels. *Anal. Chem.* **2001**, *73* (11), 2509–2515. https://doi.org/10.1021/ac001509f.
500   (24) Herr, A. E.; Molho, J. I.; Santiago, J. G.; Mungal, M. G.; Kenny, T. W.; Garguilo, M. G.
501   Electroosmotic Capillary Flow with Nonuniform Zeta Potential. *Anal. Chem.* **2000**, *72* (5),
502   1053–1057. https://doi.org/10.1021/ac990489i.
503   (25) Tallarek, U.; Rapp, E.; Scheenen, T.; Bayer, E.; Van As, H. Electroosmotic and Pressure-Driven
504   Flow in Open and Packed Capillaries: Velocity Distributions and Fluid Dispersion. *Anal. Chem.*
505   **2000**, *72* (10), 2292–2301. https://doi.org/10.1021/ac991303i.
506   (26) Lee, Y.-F.; Huang, Y.-F.; Tsai, S.-C.; Lai, H.-Y.; Lee, E. Electrophoretic and Electroosmotic
507   Motion of a Charged Spherical Particle within a Cylindrical Pore Filled with Debye–Bueche–
508   Brinkman Polymeric Solution. *Langmuir* **2016**, *32* (49), 13106–13115.
509   https://doi.org/10.1021/acs.langmuir.6b02795.
510   (27) Lee, T. C.; Keh, H. J. Electrophoretic Motion of a Charged Particle in a Charged Cavity. *Eur. J.*
511   *Mech. - BFluids* **2014**, *48*, 183–192. https://doi.org/10.1016/j.euromechflu.2014.06.004.
512   (28) Liu, H.; Bau, H. H.; Hu, H. H. Electrophoresis of Concentrically and Eccentrically Positioned
513   Cylindrical Particles in a Long Tube. *Langmuir* **2004**, *20* (7), 2628–2639.
514   https://doi.org/10.1021/la035849i.
515   (29) Redman, J. A.; Walker, S. L.; Elimelech, M. Bacterial Adhesion and Transport in Porous Media:
516   Role of the Secondary Energy Minimum. *Environ. Sci. Technol.* **2004**, *38* (6), 1777–1785.
517   https://doi.org/10.1021/es034887l.
518   (30) Locke, B. R. Electrophoretic Transport in Porous Media: A Volume-Averaging Approach. *Ind.*
519   *Eng. Chem. Res.* **1998**, *37* (2), 615–625.
520   (31) Pennathur, S.; Santiago, J. G. Electrokinetic Transport in Nanochannels. 1. Theory. *Anal. Chem.*
521   **2005**, *77* (21), 6772–6781. https://doi.org/10.1021/ac050835y.
522   (32) Johnson, P. R.; Sun, N.; Elimelech, M. Colloid Transport in Geochemically Heterogeneous
523   Porous Media: Modeling and Measurements. *Environ. Sci. Technol.* **1996**, *30* (11), 3284–3293.
524   https://doi.org/10.1021/es960053+.
525   (33) Bhattacharjee, S.; Ko, C.-H.; Elimelech, M. DLVO Interaction between Rough Surfaces.
526   *Langmuir* **1998**, *14* (12), 3365–3375. https://doi.org/10.1021/la971360b.
527   (34) Schofield, A. L.; Rudd, T. R.; Martin, David. S.; Fernig, D. G.; Edwards, C. Real-Time
528   Monitoring of the Development and Stability of Biofilms of Streptococcus Mutans Using the
529   Quartz Crystal Microbalance with Dissipation Monitoring. *Biosens. Bioelectron.* **2007**, *23* (3),
530   407–413. https://doi.org/10.1016/j.bios.2007.05.001.
531   (35) Herzberg, M.; Sweity, A.; Brami, M.; Kaufman, Y.; Freger, V.; Oron, G.; Belfer, S.; Kasher, R.
532   Surface Properties and Reduced Biofouling of Graft-Copolymers That Possess Oppositely
533   Charged Groups. *Biomacromolecules* **2011**, *12* (4), 1169–1177.
534   https://doi.org/10.1021/bm101470y.
535   (36) Olsson, A. L. J.; van der Mei, H. C.; Busscher, H. J.; Sharma, P. K. Acoustic Sensing of the
536   Bacterium–Substratum Interface Using QCM-D and the Influence of Extracellular Polymeric
537   Substances. *J. Colloid Interface Sci.* **2011**, *357* (1), 135–138.
538   https://doi.org/10.1016/j.jcis.2011.01.035.
539   (37) Strauss, J.; Liu, Y.; Camesano, T. A. Bacterial Adhesion to Protein-Coated Surfaces: An AFM
540   and QCM-D Study. *JOM J. Miner. Met. Mater. Soc.* **2009**, *61* (9), 71–74.

541 (38) Jiang, D.; Li, B.; Jia, W.; Lei, Y. Effect of Inoculum Types on Bacterial Adhesion and Power
542   Production in Microbial Fuel Cells. *Appl. Biochem. Biotechnol.* **2010**, *160* (1), 182–196.
543   https://doi.org/10.1007/s12010-009-8541-z.
544 (39) Camesano, T. A.; Liu, Y.; Datta, M. Measuring Bacterial Adhesion at Environmental Interfaces
545   with Single-Cell and Single-Molecule Techniques. *Adv. Water Resour.* **2007**, *30* (6–7), 1470–
546   1491. https://doi.org/10.1016/j.advwatres.2006.05.023.
547 (40) Fredriksson, C.; Kihlman, S.; Rodahl, M.; Kasemo, B. The Piezoelectric Quartz Crystal Mass
548   and Dissipation Sensor: A Means of Studying Cell Adhesion. *Langmuir* **1998**, *14* (2), 248–251.
549   https://doi.org/10.1021/la9710005l.
550 (41) Feiler, A. A.; Sahlholm, A.; Sandberg, T.; Caldwell, K. D. Adsorption and Viscoelastic
551   Properties of Fractionated Mucin (BSM) and Bovine Serum Albumin (BSA) Studied with
552   Quartz Crystal Microbalance (QCM-D). *J. Colloid Interface Sci.* **2007**, *315* (2), 475–481.
553   https://doi.org/10.1016/j.jcis.2007.07.029.
554 (42) Olsson, A. L. J.; van der Mei, H. C.; Busscher, H. J.; Sharma, P. K. Novel Analysis of
555   Bacterium−Substratum Bond Maturation Measured Using a Quartz Crystal Microbalance.
556   *Langmuir* **2010**, *26* (13), 11113–11117. https://doi.org/10.1021/la100896a.
557 (43) Qi, M.; Gong, X.; Wu, B.; Zhang, G. Landing Dynamics of Swimming Bacteria on a Polymeric
558   Surface: Effect of Surface Properties. *Langmuir* **2017**, *33* (14), 3525–3533.
559   https://doi.org/10.1021/acs.langmuir.7b00439.
560 (44) Song, L.; Sjollema, J.; Sharma, P. K.; Kaper, H. J.; van der Mei, H. C.; Busscher, H. J.
561   Nanoscopic Vibrations of Bacteria with Different Cell-Wall Properties Adhering to Surfaces
562   under Flow and Static Conditions. *ACS Nano* **2014**, *8* (8), 8457–8467.
563   https://doi.org/10.1021/nn5030253.
564 (45) Gutman, J.; Walker, S. L.; Freger, V.; Herzberg, M. Bacterial Attachment and Viscoelasticity:
565   Physicochemical and Motility Effects Analyzed Using Quartz Crystal Microbalance with
566   Dissipation (QCM-D). *Environ. Sci. Technol.* **2013**, *47* (1), 398–404.
567   https://doi.org/10.1021/es303394w.
568 (46) Tarnapolsky, A.; Freger, V. Modeling QCM-D Response to Deposition and Attachment of
569   Microparticles and Living Cells. *Anal. Chem.* **2018**, *90* (23), 13960–13968.
570   https://doi.org/10.1021/acs.analchem.8b03411.
571 (47) Marcus, I. M.; Herzberg, M.; Walker, S. L.; Freger, V. Pseudomonas Aeruginosa Attachment on
572   QCM-D Sensors: The Role of Cell and Surface Hydrophobicities. *Langmuir* **2012**, *28* (15),
573   6396–6402. https://doi.org/10.1021/la300333c.
574 (48) Tanner, F. W. *Shape and Size of Bacterial Cells: Bacteriology*; John Wiley and Sons, Inc., New
575   York, 1948.
576 (49) Nelson, K. E.; Weinel, C.; Paulsen, I. T.; Dodson, R. J.; Hilbert, H.; Martins dos Santos, V. A.
577   P.; Fouts, D. E.; Gill, S. R.; Pop, M.; Holmes, M. Complete Genome Sequence and Comparative
578   Analysis of the Metabolically Versatile Pseudomonas Putida KT2440. *Environ. Microbiol.*
579   **2002**, *4* (12), 799–808.
580 (50) Foght, J. M.; Westlake, D. W. Transposon and Spontaneous Deletion Mutants of Plasmid-Borne
581   Genes Encoding Polycyclic Aromatic Hydrocarbon Degradation by a Strain of Pseudomonas
582   Fluorescens. *Biodegradation* **1996**, *7* (4), 353–366.
583 (51) Ghanem, N.; Kiesel, B.; Kallies, R.; Harms, H.; Chatzinotas, A.; Wick, L. Y. Marine Phages As
584   Tracers: Effects of Size, Morphology, and Physico–Chemical Surface Properties on Transport in
585   a Porous Medium. *Environ. Sci. Technol.* **2016**, *50* (23), 12816–12824.
586   https://doi.org/10.1021/acs.est.6b04236.
587 (52) Hermansson, M. The DLVO Theory in Microbial Adhesion. *Colloids Surf. B Biointerfaces*
588   **1999**, *14* (1), 105–119.
589 (53) *Particle Deposition and Aggregation: Measurement, Modelling and Simulation*; Elimelech, M.,
590   Ed.; Colloid and surface engineering series; Butterworth-Heinemann: Oxford, 1998.
591 (54) Probstein, R. F. *Physicochemical Hydrodynamics: An Introduction*; John Wiley & Sons, 2005.
592 (55) Song, L.; Johnson, P. R.; Elimelech, M. Kinetics of Colloid Deposition onto Heterogeneously
593   Charged Surfaces in Porous Media. *Environ. Sci. Technol.* **1994**, *28* (6), 1164–1171.

594 (56) Simoni, S. F.; Bosma, T. N. P.; Harms, H.; Zehnder, A. J. B. Bivalent Cations Increase Both the
595   Subpopulation of Adhering Bacteria and Their Adhesion Efficiency in Sand Columns. *Environ.*
596   *Sci. Technol.* **2000**, *34* (6), 1011–1017. https://doi.org/10.1021/es990476m.
597 (57) Rijnaarts, H. H. *Interactions between Bacteria and Solid Surfaces in Relation to Bacterial*
598   *Transport in Porous Media.*
599 (58) Rijnaarts, H. H. M.; Norde, W.; Bouwer, E. J.; Lyklema, J.; Zehnder, A. J. B. Reversibility and
600   Mechanism of Bacterial Adhesion. *Colloids Surf. B Biointerfaces* **1995**, *4* (1), 5–22.
601   https://doi.org/10.1016/0927-7765(94)01146-V.
602 (59) Tufenkji, N.; Elimelech, M. Breakdown of Colloid Filtration Theory: Role of the Secondary
603   Energy Minimum and Surface Charge Heterogeneities. *Langmuir* **2005**, *21* (3), 841–852.
604   https://doi.org/10.1021/la048102g.
605 (60) Ward, M. D.; Buttry, D. A. In Situ Interfacial Mass Detection with Piezoelectric Transducers.
606   *Science* **1990**, *249* (4972), 1000–1007.
607 (61) Reviakine, I.; Johannsmann, D.; Richter, R. P. Hearing What You Cannot See and Visualizing
608   What You Hear: Interpreting Quartz Crystal Microbalance Data from Solvated Interfaces. *Anal.*
609   *Chem.* **2011**, *83* (23), 8838–8848. https://doi.org/10.1021/ac201778h.
610 (62) Sauerbrey, G. Verwendung von Schwingquarzen zur Wägung dünner Schichten und zur
611   Mikrowägung. *Z. Für Phys.* **1959**, *155* (2), 206–222. https://doi.org/10.1007/BF01337937.
612 (63) Kao, W.-L.; Chang, H.-Y.; Lin, K.-Y.; Lee, Y.-W.; Shyue, J.-J. Effect of Surface Potential on
613   the Adhesion Behavior of NIH3T3 Cells Revealed by Quartz Crystal Microbalance with
614   Dissipation Monitoring (QCM-D). *J. Phys. Chem. C* **2017**, *121* (1), 533–541.
615   https://doi.org/10.1021/acs.jpcc.6b11217.
616 (64) Simoni, S. F.; Harms, H.; Bosma, T. N. P.; Zehnder, A. J. B. Population Heterogeneity Affects
617   Transport of Bacteria through Sand Columns at Low Flow Rates. *Environ. Sci. Technol.* **1998**,
618   *32* (14), 2100–2105. https://doi.org/10.1021/es970936g.
619 (65) de la Guardia, M.; Garrigues, S. *Handbook of Green Analytical Chemistry*; John Wiley & Sons,
620   2012.
621 (66) König, S.; Worrich, A.; Banitz, T.; Centler, F.; Harms, H.; Kästner, M.; Miltner, A.; Wick, L.
622   Y.; Thullner, M.; Frank, K. Spatiotemporal Disturbance Characteristics Determine Functional
623   Stability and Collapse Risk of Simulated Microbial Ecosystems. *Sci. Rep.* **2018**, *8* (1), 9488.
624 (67) König, S.; Worrich, A.; Banitz, T.; Harms, H.; Kästner, M.; Miltner, A.; Wick, L. Y.; Frank, K.;
625   Thullner, M.; Centler, F. Functional Resistance to Recurrent Spatially Heterogeneous
626   Disturbances Is Facilitated by Increased Activity of Surviving Bacteria in a Virtual Ecosystem.
627   *Front. Microbiol.* **2018**, *9*, 734.
628 (68) Shan, Y.; Qin, J.; Harms, H.; Wick, L. Y. Electrokinetic Effects on the Interaction of
629   Phenanthrene with Geo-Sorbents. *Chemosphere* **2019**, 125161.
630 (69) Qin, J.; Moustafa, A.; Harms, H.; El-Din, M. G.; Wick, L. Y. The Power of Power:
631   Electrokinetic Control of PAH Interactions with Exfoliated Graphite. *J. Hazard. Mater.* **2015**,
632   *288*, 25–33. https://doi.org/10.1016/j.jhazmat.2015.02.008.
633